Title

Acquired stress resilience through bacteria-to-nematode interdomain horizontal gene transfer.

Permalink

Journal

The EMBO Journal, 42(24)

Authors

Pandey, Taruna

Kalluraya, Chinmay

Wang, Bingying

et al.

Publication Date

2023-12-11

DOI

SOURCE DATA

TRANSPARENT PROCESS

THE EMBO JOURNAL

Acquired stress resilience through bacteria-to-nematode interdomain horizontal gene transfer

Taruna Pandey[1],[†], Chinmay A Kalluraya[2],[†] iD, Bingying Wang[1], Ting Xu[3], Xinya Huang[3], Shouhong Guang[3] iD, Matthew D Daugherty[2],[*] iD & Dengke K Ma[1],[4],[**] iD

Abstract

Natural selection drives the acquisition of organismal resilience traits to protect against adverse environments. Horizontal gene transfer (HGT) is an important evolutionary mechanism for the acquisition of novel traits, including metazoan acquisitions in immunity, metabolic, and reproduction function via interdomain HGT (iHGT) from bacteria. Here, we report that the nematode gene *rml-3* has been acquired by iHGT from bacteria and that it enables exoskeleton resilience and protection against environmental toxins in *Caenorhabditis elegans*. Phylogenetic analysis reveals that diverse nematode RML-3 proteins form a single monophyletic clade most similar to bacterial enzymes that biosynthesize L-rhamnose, a cell-wall polysaccharide component. *C. elegans rml-3* is highly expressed during larval development and upregulated in developing seam cells upon heat stress and during the stress-resistant dauer stage. *rml-3* deficiency impairs cuticle integrity, barrier functions, and nematode stress resilience, phenotypes that can be rescued by exogenous L-rhamnose. We propose that interdomain HGT of an ancient bacterial *rml-3* homolog has enabled L-rhamnose biosynthesis in nematodes, facilitating cuticle integrity and organismal resilience to environmental stressors during evolution. These findings highlight a remarkable contribution of iHGT on metazoan evolution conferred by the domestication of a bacterial gene.

Introduction

Genetic information is primarily transmitted vertically from parents to offspring through sexual or asexual reproduction. However, genes can also be transmitted from one organism to a non-offspring organism via horizontal gene transfer (HGT). While HGT is widespread among bacteria, interdomain HGT (iHGT) between bacteria and eukaryotes is less common. In particular, iHGT from bacteria into metazoans is expected to be very rare, as long-term functional acquisition requires a transferred bacterial gene to integrate into a metazoan germline, followed by subsequent gene expression and a selective benefit to the recipient metazoan during evolution. Despite this expected rarity, cases of iHGT have been strongly suggested by phylogenetic analysis for several lineage-specific metazoan functions (Dunning Hotopp, 2011; Zhaxybayeva & Doolittle, 2011; Crisp *et al*, 2015; Husnik & McCutcheon, 2018). Examples include metazoan domestication of bacterial genes that allow nutrient intake, metabolic functions, reproductive behaviors and immune functions that confer defense against pathogens and predators (Scholl *et al*, 2003; Danchin *et al*, 2010; Ferguson *et al*, 2011; Mayer *et al*, 2011; Pauchet & Heckel, 2013; Schönknecht *et al*, 2013; Wheeler *et al*, 2013; Metcalf *et al*, 2014; Wybouw *et al*, 2014; Chou *et al*, 2015; Luan *et al*, 2015; Schiffer *et al*, 2019; Verster *et al*, 2019; Morehouse *et al*, 2020; Bernheim *et al*, 2021; Kalluraya *et al*, 2023).

Nematodes are the most abundant species of metazoans on Earth and crucial members of terrestrial ecosystems (Blaxter *et al*, 1998; Sommer & Bumbarger, 2012; Haag *et al*, 2018; van den Hoogen *et al*, 2019). In nature, nematodes occupy diverse ecological niches and consequently evolved many unique strategies to survive under conditions of adverse environmental stresses. For example, nematodes can deploy remarkable plasticity by shifting to the dauer stage of reproductive arrest during unfavorable environmental conditions

1 Cardiovascular Research Institute and Department of Physiology, University of California San Francisco, San Francisco, CA, USA
2 Department of Molecular Biology, University of California, San Diego, CA, USA
3 Division of Life Sciences and Medicine, Department of Obstetrics and Gynecology, The USTC RNA Institute, Ministry of Education Key Laboratory for Membraneless Organelles & Cellular Dynamics, School of Life Sciences, The First Affiliated Hospital of USTC, Biomedical Sciences and Health Laboratory of Anhui Province, University of Science and Technology of China, Hefei, China
4 Innovative Genomics Institute, University of California, Berkeley, CA, USA
   *Corresponding author. Tel: 858 534 1292; E-mail: mddaugherty@ucsd.edu
   **Corresponding author. Tel: 857 230 5323; E-mail: dengke.ma@ucsf.edu
   †These authors contributed equally to this work

and entering anhydrobiosis to survive extreme desiccation (Fielenbach & Antebi, 2008; McGill *et al*, 2015). Nematode genomes encode many enzymes that function to detoxify environmental toxins and genetic programs that enhance resilience to specific environmental stresses (Rodriguez *et al*, 2013; Wang *et al*, 2022). In addition, nematodes withstand harsh environments physically aided by the exoskeleton, with specialized layers of cuticle that form the barrier between the animal and its environment (Johnstone, 1994). In the cuticle, extracellular matrix biomolecules can be extensively cross-linked (e.g. by collagen) and modified by various types of lipid- and glycan-conjugates to enable cuticle integrity and barrier functions.

Nematodes are also unique among known metazoans in that they encode an L-rhamnose biosynthetic pathway. This pathway is widespread in prokaryotes and plants, where L-rhamnose forms the constituent of lipopolysaccharide (LPS) of diverse bacteria (Mistou *et al*, 2016), the cell wall and specialized metabolites of plants (Jiang *et al*, 2021), and the cell wall of pathogenic fungi (Martinez *et al*, 2012). Strikingly, among metazoans, the production of L-rhamnose has only been described in nematodes through the activities of four separate enzymes, RML-1 through RML-4, which are expressed during the formation of the *Caenorhabditis elegans* cuticle (Feng *et al*, 2016). Nonetheless, the evolutionary origins and functional relevance of key enzymes in the nematode-specific L-rhamnose pathway remained unresolved.

In this work, we used phylogenetic methods to demonstrate that one of the key enzymes of the nematode L-rhamnose biosynthetic pathway, RML-3, arose from an iHGT event from bacteria. We identified RML-3 protein sequences in a diverse range of nematodes that form a single highly supported monophyletic clade most similar to bacterial dTDP-4-dehydrorhamnose-3-5-epimerase enzymes based on multiple phylogenetic reconstruction methods. In the model organism nematode *C. elegans*, we found that *rml-3* is expressed and dynamically regulated by stress in developing seam cells and hypoderm. Functional analyses revealed the critical roles of RML-3 in cuticle integrity, supporting the evolutionarily acquired L-rhamnose biosynthetic capacity in nematodes and exoskeleton stress resilience through iHGT from bacteria.

Results

Nematodes acquired a bacteria-derived gene in the L-rhamnose biosynthetic pathway

To understand the atypical phylogenetic distribution of the L-rhamnose biosynthetic pathway across the tree of life, we searched for patterns of conservation among each constituent enzyme. In plants and fungi, L-rhamnose is produced via the UDP pathway,

while in bacteria and nematodes, the RML pathway leads to the biosynthesis of L-rhamnose (Fig 1A) (Giraud & Naismith, 2000). Notably, RML-3 is the only enzyme in the L-rhamnose pathway that is found in nematodes but appears to be absent in other eukaryotes. To learn more about the evolutionary origins of RML-3, we performed a BLASTP search to obtain all available homologous sequences from the RefSeq database using the *C. elegans* RML-3 protein sequence (accession NP_509046.1). Outside nematodes, the next most closely related sequences ordered by the BLASTP bit-score (S) probability (*e*-value) were identified in bacterial and archaeal genomes (Dataset EV1). In the highly conserved bacterial homologs, RML-3 is a dTDP-4-dehydrorhamnose 3,5-epimerase that catalyzes the third step in L-rhamnose biosynthesis from glucose-1-phosphate (Fig 1A) (Mistou *et al*, 2016). To increase our sampling of nematodes, we also queried the non-redundant (NR), whole-genome sequencing (WGS), and transcriptome (TSA) databases. These searches revealed RML-3 homologs in a wide range of species in the *Chromadoria* clade of nematodes, which includes both free-living (e.g. *C. elegans*) as well as parasitic (e.g. *Enterobius vermicularis*) nematodes (Fig EV1, Dataset EV1) (Smythe *et al*, 2019). In contrast, we found no RML-3 homologs in well-sequenced members of the *Dorylaimia* clade of nematodes (e.g. *Trichinella spiralis*) (Fig EV1). Based on this, we infer that nematode RML-3 was horizontally acquired from bacteria after the divergence of the *Chromadoria* and *Dorylaimia* clades, which is estimated to have occurred > 400 million years ago (Rota-Stabelli *et al*, 2013; Smythe *et al*, 2019).

To confirm the bacterial origin of nematode RML-3, we reconstructed a maximum likelihood (ML) phylogenetic tree using available RML-3 protein sequences from prokaryotes and metazoans (Fig 1B, Datasets EV1 and EV2). Our phylogenetic analyses reveal that nematode RML-3 forms a single monophyletic clade with high-branch support, nested within a larger group of bacterial sequences. The monophyly of the nematode clade is maintained irrespective of the choice of ML phylogenetic reconstruction software or substitution model (Fig EV2, Dataset EV2). The most closely related bacterial species in all analyses are members of the *Chlamydiales* order of bacteria, which are obligate intracellular bacteria (Elwell *et al*, 2016; Bayramova *et al*, 2018) (Figs 1B and EV2). These data suggest that intracellular *Chlamydiales* bacteria were likely the "donor" species for RML-3, although caution should be taken given our inference that this gene transfer event occurred > 400 million years ago (Rota-Stabelli *et al*, 2013) and there have likely been subsequent evolution that has taken place in bacterial and nematode genomes that may complicate inferences of an exact "donor".

Over the period of *rml-3* gene domestication, nematodes acquired four introns within the horizontally transferred *rml-3* coding region (Fig 1C). Nematode RML-3 homologs also show similar patterns of amino acid conservation as seen in bacterial enzymes, including

Figure 1. Nematodes acquired an enzyme required for L-rhamnose sugar biosynthesis by iHGT.

A L-rhamnose biosynthetic pathway with reaction intermediates and differences in the conservation of enzymes across domains of life. The presence of homologs of the *C. elegans* RML-3 enzyme and production of dTDP-L-rhamnose is unique to bacteria and nematodes (orange).

B Maximum-likelihood phylogenetic tree of RML-3 proteins and bacterial homologs. Relevant bootstrap branch support values > 90 are indicated by asterisks or numbers. Scale bar shows the estimated divergence in amino acid changes per residue. A complete phylogenetic tree with support values is found in Dataset EV2.

C Schematic genomic locus architecture of RML-3 homologs in *C. elegans* (RML-3) and *Protochlamydia sp. R18* (*rfbC*). Red carets within *C. elegans* genes represent introns.

D Consensus sequence and positions of the predicted catalytic residues (yellow) for RML-3 homologs are shown in (B). Four bacterial sequences are shown, including from three representative bacteria (*Salmonella enterica*, *C. perfringens*, and *Pseudomonas aeruginosa*) and an example from the clade of putative iHGT donor bacteria, *Candidatus Protochlamydia* sp. R18, as well as four representative nematode sequences. Amino acid numbering corresponds to the *S. enterica* and *C. elegans* proteins respectively.

Figure 1.

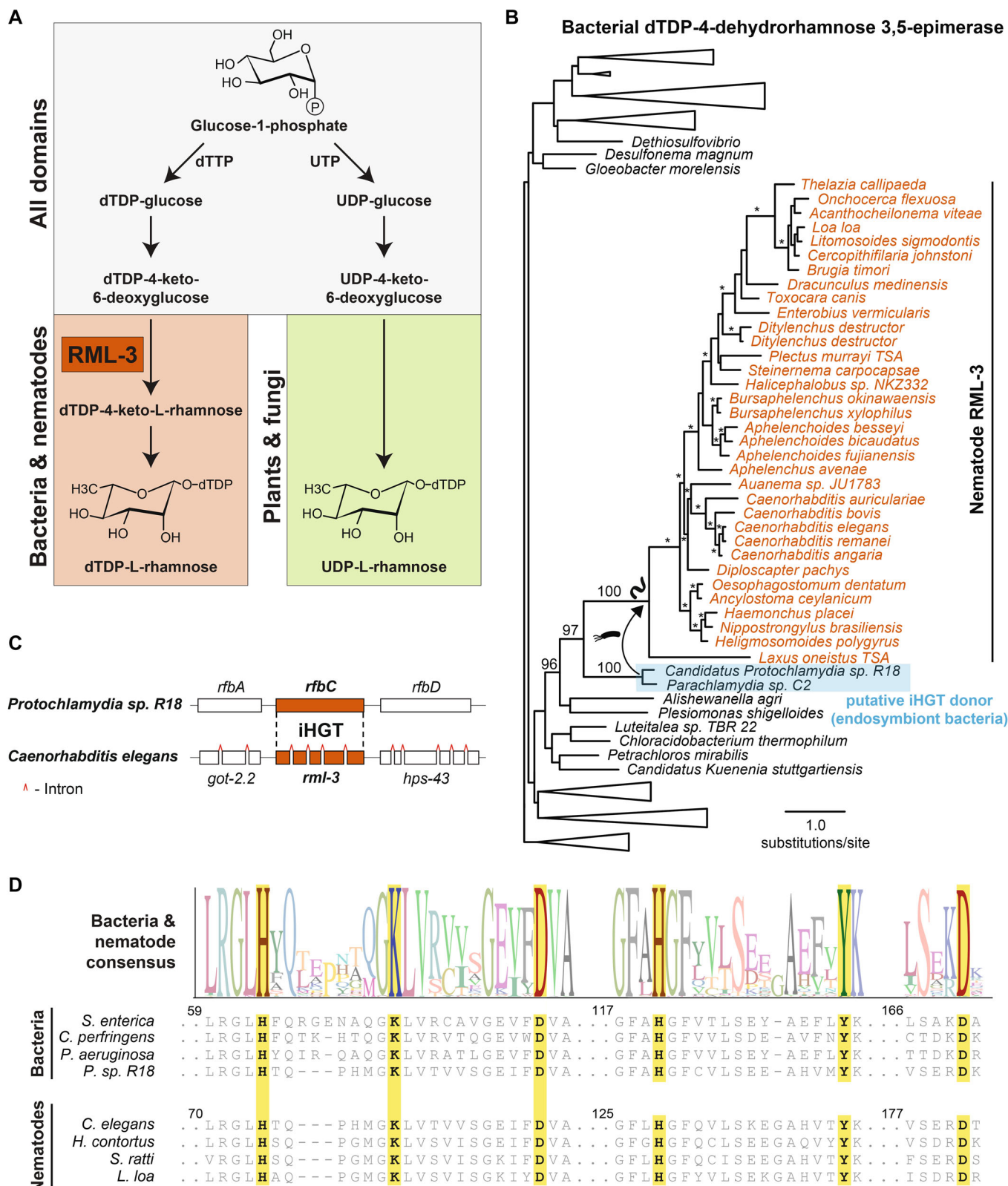retention of critical catalytic residues (Fig 1D) (Giraud & Naismith, 2000), which is consistent with the described epimerase catalytic activity (Feng *et al*, 2016) of *C. elegans* RML-3. Importantly, RML-3

lacks similarity to the enzyme that catalyzes the epimerase reaction in plants and fungi, which is part of a bifunctional or trifunctional enzyme that catalyzes the last two steps in the biosynthetic pathway

that results in UDP-L-rhamnose (Fig 1A). Together, these data indicate that nematodes acquired an essential enzyme in L-rhamnose biosynthesis by iHGT from bacteria.

rml-3 expression pattern and regulation during development, dauer, and stress

To gain a deeper understanding of the fascinating evolutionary acquisition of RML-3 from bacteria through iHGT, and its physiological relevance in modern nematodes, we characterized the expression, regulation, and biological functions of RML-3 in the tractable model organism nematode *C. elegans*.

We first generated an integrated transgene-based transcriptional reporter, *rml-3*p::GFP, and CRISPR-mediated GFP knock-in (KI) alleles at the endogenous *rml-3* locus (Figs 2 and EV3). The *rml-3* transcriptional reporter showed specific *rml-3* expression in the hypoderm (primarily in the seam cells, and less abundantly in the Hyp7) during larval development, starting from larval L1 through L4 and young adult (24 h post L4) stages (Fig 2A–D). Seam cells, also referred to as lateral hypodermal cells, share functions with the major hypodermis in secreting biomolecules to form the cuticle in *C. elegans* (Johnstone, 1994). In dauer animals, we observed *rml-3* expression predominantly in the hypodermal syncytium as seam cells were dramatically shrunk (Fig 2E). The CRISPR GFP knock-in alleles showed identical expression patterns as the transcriptional reporter during late embryonic and larval development, albeit with lower overall fluorescence intensity of the knock-in reporter (Fig EV3). In mature adult animals (> 48 h post L4), we observed no detectable *rml-3* expression from either transcriptional or endogenous *rml-3* knock-in GFP reporters.

To examine the regulation of *rml-3* by environmental stress, we exposed *rml-3*p::GFP animals to various types of stress (hypoxia, anoxia, hypothermia, freezing, heat, and osmotic shock). We found that only heat shock at various degrees and durations caused markedly increased expression of *rml-3* in seam cells, accompanied by rounded seam cell morphology (Fig 2F–J). We used RNAi of several candidate genes (*hsf-1*, *hif-1*, *nhr-49*, *skn-1*, *daf-16*, *sta-2*) encoding known stress-responding transcription factors to probe the mechanism of *rml-3* regulation by heat stress (Rodriguez *et al*, 2013; Ma *et al*, 2015; Brunquell *et al*, 2016; Jiang *et al*, 2018). Among the candidate genes tested, we observed that *nhr-49* (nuclear hormone receptor) RNAi strongly suppressed *rml-3* upregulation by heat (Fig 2K). However, this effect is likely indirect as we did not find evidence for direct binding of NHR-49 to the *rml-3* promoter (ModENCODE). Taken together, our expression analyses reveal specific baseline expression of *rml-3* in the developing seam cells, rapid upregulation by heat stress, and expression in the dauer hypoderm. As NHR-49 regulates pleiotropic stress-dependent genetic programs (Taubert *et al*, 2008; Vozdek *et al*, 2018; Dasgupta *et al*, 2020; Naim *et al*, 2021), we sought to probe specific biological functions of RML-3 using *rml-3* RNAi, which strongly decreased endogenous *rml-3*::GFP expression in the CRISPR KI strain (Fig 2L).

Rml-3 RNAi impairs cuticle integrity and epithelial barrier functions

The *C. elegans* cuticle is structured as dorsal and ventral regions covering the broad dorsal and ventral hypodermis and the narrow lateral regions overlying the seam cells (Johnstone, 1994). The cuticle is synthesized at the end of embryogenesis and in five cycles prior to each larval stage. The seam cell and hypodermal expression pattern of *rml-3* led us to examine the functional roles of RML-3 in cuticle formation and integrity. Toward this, we tested the effect of *rml-3* RNAi using a GFP reporter of COL-19, a secreted collagen protein critical for the exoskeleton structure of the cuticle (Thein *et al*, 2003; Zhang *et al*, 2021, Zhang *et al*, 2020). The COL-19::GFP reporter is abundant along the annular furrows and lateral alae in the cuticle under normal conditions (Fig 3A). RNAi of several genes involved in collagen synthesis, including *dpy-7*, *dpy-11*, *sqt-1*, *rol-6*, *bli-1* have been previously reported to cause disruption, branching, and amorphous state changes in lateral alae and annuli leading to morphological defects labeled by COL-19::GFP (Thein *et al*, 2003). We found that both *rml-1* and *rml-3* RNAi caused amorphous lateral alae and disrupted annuli, frequently accompanied by severe hole-like cuticle defects, as revealed in COL-19::GFP animals (Fig 3A and B).

The integrity of the cuticle is vital for barrier functions and protection against environmental toxins in *C. elegans*. Mutations of *rml-2*, also known as *bus-5*, led to impaired cuticle-barrier functions and sensitivity to boric acid (BA), a chemical present in nature and as an insecticide that imposes organismal toxicity (Kiesche-Nesselrodt & Hooser, 1990; Gravato-Nobre *et al*, 2005; Xiong *et al*, 2017). Hence, we next assessed the BA sensitivity of animals treated with *rml-3* RNAi. We found that low-dose exposure to BA (6 mM in medium) caused a robust developmental delay in animals with *rml-3* RNAi (Fig 3C). Moreover, high-dose exposure to BA (20 mM) caused a dramatic reduction in the survival of animals with *rml-3* RNAi compared to control (Fig 3D), demonstrating an essential role of RML-3 in protection against the BA toxin.

To further characterize the effect of *rml-3* RNAi on cuticle integrity, we used an integrated transcriptional reporter *nlp-29*p::GFP. *nlp-29* encodes an antimicrobial peptide reported to increase in expression under conditions of hypodermal infection, wounds, or disrupted cuticle in *C. elegans* (Pujol *et al*, 2008; Sinner *et al*, 2021; Chandler & Choe, 2022). We found that *rml-3* RNAi strongly increased *nlp-29*p::GFP expression both during late larval development (L4) and in young adults (24 h post-L4) (Fig 3E). Consistently, RNAi against *rml-2* (also known as *bus-5*) also markedly increased *nlp-29*p::GFP expression (Fig EV4). Using a different collagen GFP reporter DPY-7::GFP, we observed additional cuticle defects in animals treated with *rml-3* RNAi characterized by DPY-7::GFP aggregation and abnormal alae (Fig EV5). Given the striking similarity and homology of RML-3 to bacterial enzymes for L-rhamnose biosynthesis, we reasoned that *rml-3* RNAi caused cuticle defects resulting from reduced biosynthesis of L-rhamnose. If so, defects caused by *rml-3* RNAi could be rescued by supplementation with L-rhamnose, which can be converted to dTDP-L-rhamnose by ubiquitously expressed nucleotidyltransferases (Li *et al*, 2022). Indeed, we found that exogenously provided L-rhamnose partially rescued the hole-like cuticle defect of animals with *rml-3* RNAi (Fig 3F and G). In addition, *rml-3* RNAi caused reduced resistance to heat stress (Fig EV5B and C), a phenotype also rescued by exogenous L-rhamnose (Fig EV5C). These results indicate that *rml-3* is crucial for the L-rhamnose biosynthetic pathway, which in turn is necessary to maintain proper cuticle organization and stress resilience against adverse environmental stresses.
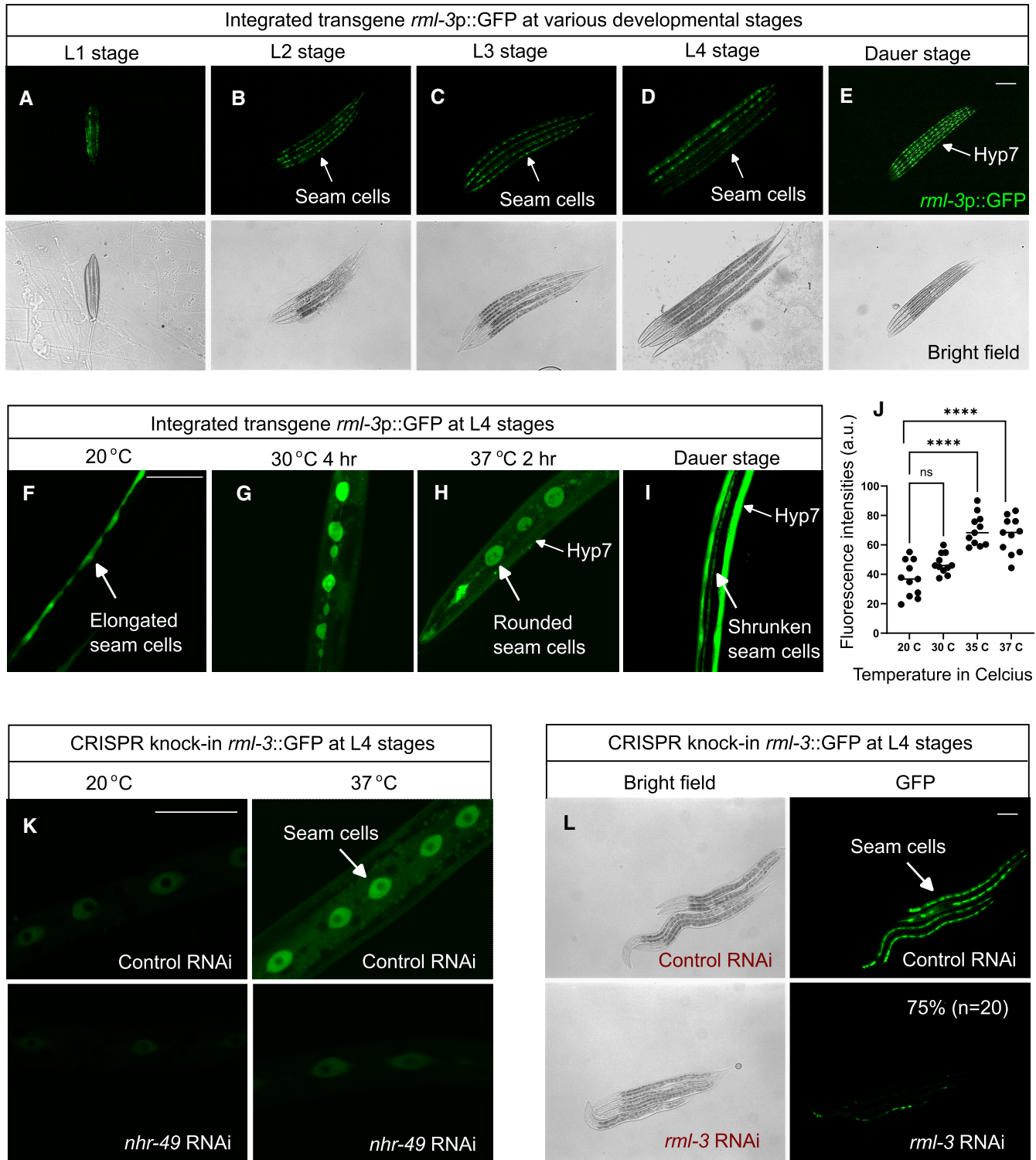
Figure 2. ***Caenorhabditis elegans rml-3* expression pattern and regulation in development, dauer, and stress responses..**

A–E   Transcriptional GFP reporters showing *rml-3* expression patterns during larval development and in dauer-stage animals.

F–J   Transcriptional GFP reporters showing *rml-3* expression patterns after heat stress and heat-induced dauer formation, with quantification of GFP induction and statistical analysis (J) by Dunnett's multiple comparisons tests (****$P < 0.0001$; ns, not significant).

K   CRISPR-mediated RML-3::GFP KI reporters show *rml-3* expression in seam cells and induction by heat (37°C for 2 h) in an NHR-49-dependent manner.

L   *rml-3* RNAi abolishes RML-3::GFP expression in KI reporters. Scale bars: 100 μm.

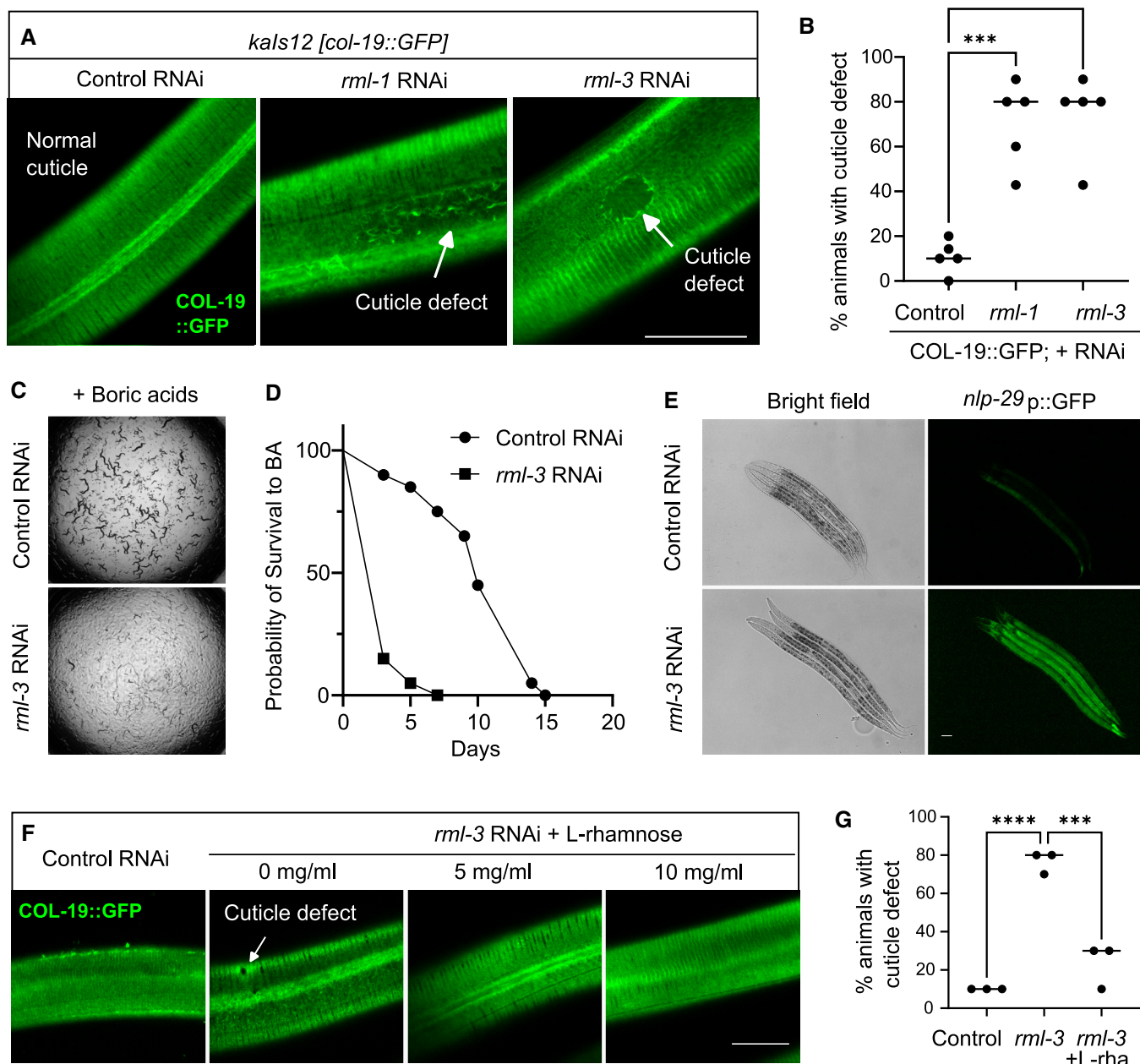Source data are available online for this figure.

Figure 3. *rml-3* RNAi impairs cuticle integrity and epithelial barrier functions in *C. elegans*.

A Representative confocal images showing cuticle hole defects caused by RNAi against *rml-1* or *rml-3* visualized by the collagen COL-19::GFP reporter.

B Quantification of percentages of animals with cuticle defects (amorphous lateral alae or disrupted annuli), with statistical analysis by Dunn's multiple comparisons tests (****$P < 0.0001$; *** indicates $P < 0.001$; $N = 5$ independent experiments).

C Representative wild-field images showing boric acid (BA) sensitivity of animals treated with RNAi against *rml-3*.

D Survival curves showing accelerated death of animals ($n > 50$) treated with RNAi against *rml-3* under BA supplementation conditions. The animals were from a single experiment representative of three trials.

E Representative epifluorescence images showing upregulation of *nlp-29*p::GFP caused by RNAi against *rml-3*.

F Cuticle defects of animals with *rml-3* RNAi dose-dependently rescued by exogenous L-rhamnose.

G Quantification of rescue by L-rhamnose of the cuticle defect (amorphous lateral alae or disrupted annuli) in animals with RNAi against *rml-3*, with statistical analysis by Dunn's multiple comparisons tests (****$P < 0.0001$; *** indicates $P < 0.001$; $N = 3$ independent experiments). Scale bars: 50 μm.
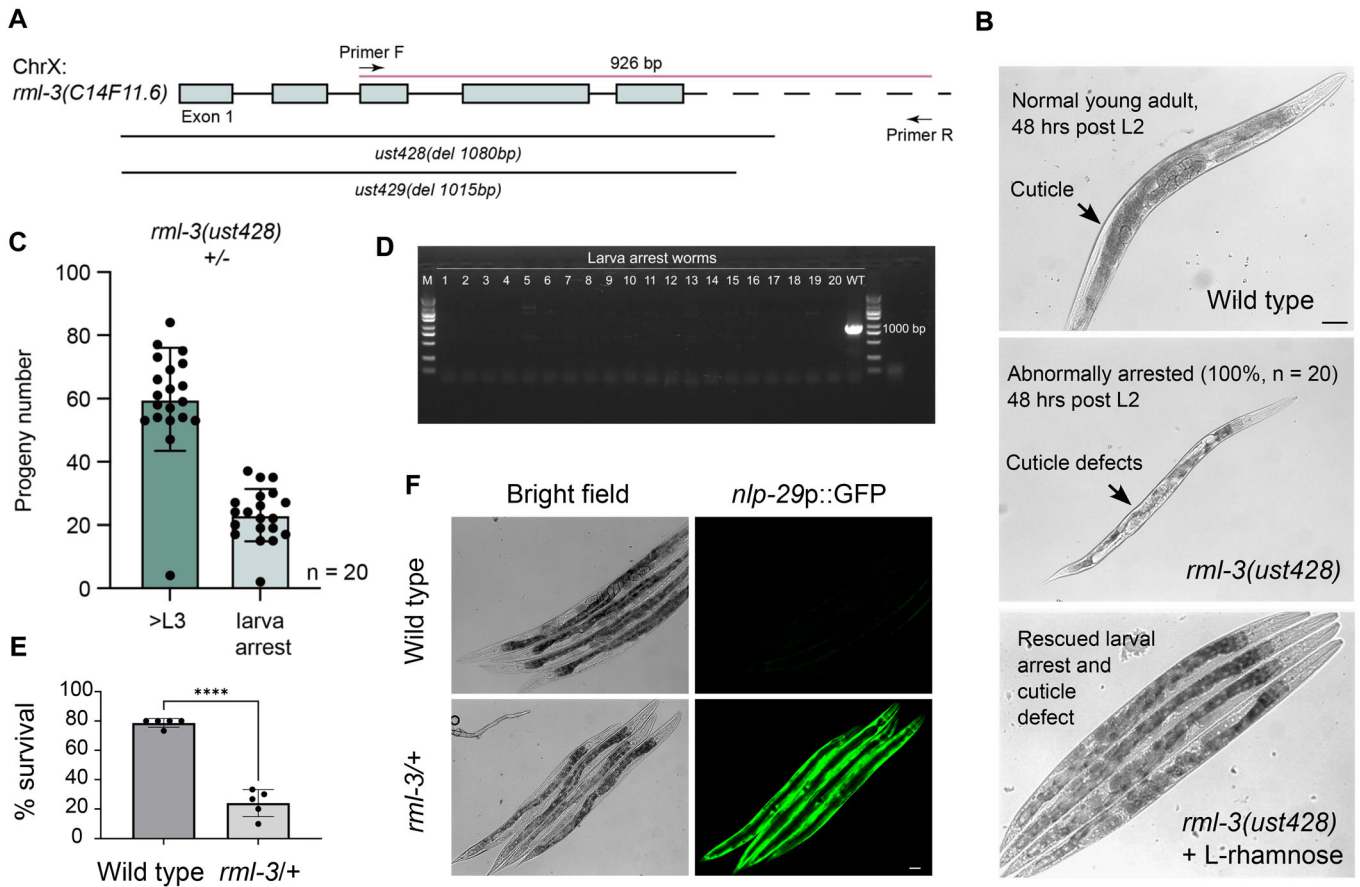
Source data are available online for this figure.

Figure 4. RML-3 ensures normal development with intact cuticle and promotes organismal resilience to environmental stress.

A   Schematic showing CRISPR-mediated deletions of *rml-3*.
B   Representative bright-field images showing developmental arrest of animals with homozygous deletions of *rml-3* and cuticle defects. Shown is also rescued development by exogenous supplementation of L-rhamnose (10 mg/ml in medium).
C   Quantification of the number of progeny that can progress beyond L3 or become arrested from 20 *rml-3*/+ heterozygous parents. The ratio of the wild type versus arrested larvae corresponds to the Mendelian 3:1 ratio.
D   PCR genotyping of 20 arrested larvae confirming *rml-3* homozygosity.
E   *rml-3* heterozygous deletion mutants showing reduced survival under BA, with statistical analysis by the non-parametric Mann–Whitney test (**$P < 0.01$; $N = 5$ independent experiments).
F   Representative bright-field and epifluorescence images showing *rml-3* heterozygous mutants with upregulated *nlp-29*p::GFP reporter expression. Scale bars: 50 μm.

Source data are available online for this figure.

RML-3 is essential for larval development and haploinsufficient for BA resistance

We next sought to determine the null phenotype of *rml-3* since RNAi does not eliminate gene functions. Using CRISPR/Cas9-mediated deletions, we obtained two independent alleles to remove the entire coding region of *rml-3* (Fig 4A). We found these homozygous deletion alleles caused identical larval L2-L3 developmental arrest phenotypes (Fig 4B). From 20 morphologically normal F1 self-progeny of heterozygous deletion mutants, the F2 progeny segregated with the expected 1:3 Mendelian ratio for the L2-L3 larval arrest phenotype (Fig 4C). From the self-progeny of heterozygous deletion mutants, we genotyped 20 randomly selected larval-arrested animals and found that 100% of them carry homozygous deletions (Fig 4D). Supplementation of L-rhamnose partially rescued the larval arrest phenotype of the *rml-3* homozygous mutants (Fig 4B).

Given the larval arrest phenotype of *rml-3* homozygotes, we further examined the BA sensitivity and *nlp-29*p::GFP phenotypes of *rml-3* heterozygous deletion mutants. Compared to the wild type, *rml-3*/+ animals showed activation of *nlp-29*p::GFP and markedly reduced survival under BA treatment (Fig 4E and F). Together, these results demonstrate that RML-3 is functionally important for progression through larval development through L-rhamnose production, while heterozygous *rml-3* causes a less severe developmental phenotype but marked defects in cuticle-barrier functions, leading to BA sensitivity and *nlp-29*p::GFP activation.

Discussion

Surviving unfavorable environmental conditions and stress has conferred nematodes with remarkable phenotypic plasticity that is

reflected in their genome evolution. Unlike common modes of genome evolution based on germline DNA mutations and organismal trait selection, rare iHGT can facilitate metazoan evolution by incorporating existing functional genomic material from bacteria into the genome of an animal. Here, we characterized the evolutionary origin and functional consequences of a critical L-rhamnose biosynthesis enzyme that nematodes acquired from bacteria via iHGT. Leveraging the increased availability of genome sequence data and multiple ML-based phylogenetic reconstruction methods, we can unequivocally show that RML-3 was transferred to nematodes followed by gene domestication that involved the evolution of introns and conservation of critical amino acid residues. This gene is now represented across a wide range of nematodes, including diverse members of the well-sampled *Rhabditina*, *Tylenchina*, and *Spirurina* clades of nematodes.

How did a single iHGT event facilitate the biosynthesis of L-rhamnose in nematodes? The enzymes that catalyze the first two steps of the pathway shown in Fig 1A, RML-1 (nucleotidyltransferase) and RML-2 (dehydratase) in nematodes, have homologs widely present in all domains of life, where they can contribute to other sugar biosynthetic pathways (Martinez *et al*, 2012; Mistou *et al*, 2016). Interestingly, the distribution of RML-4 homologs within eukaryotes is itself polyphyletic and is even found in eukaryotic viruses (Parakkottil Chothi *et al*, 2010), raising the possibility that it has been horizontally transferred among eukaryotes, possibly in a virus-mediated manner (Appendix Fig S1). Regardless of the mechanism of RML-4 origin in nematodes, it is clear that RML-1, RML-2, and RML-4 in nematodes are closely related to eukaryotic enzymes that perform similar functions. The acquisition of RML-3 from bacteria completes the biosynthetic pathway, enabling nematodes to generate L-rhamnose uniquely among known metazoans.

The identity of the bacterial "donor" species for RML-3, and the general mechanisms of iHGT, are poorly understood, owing to the high frequency of gene transfer within bacteria and the rarity of iHGT. Our phylogenetic analyses suggest that the bacterial "donors" of nematode-specific RML-3 belong to members of the *Chlamydiales* order of bacteria, which are obligate intracellular bacteria and stable symbionts of diverse organisms (Elwell *et al*, 2016; Bayramova *et al*, 2018). These data indicate that endosymbiosis may have facilitated the iHGT of RML-3 into nematodes, consistent with several other instances of iHGT from endosymbiont bacteria into their host species (Kondo *et al*, 2002; Dunning Hotopp *et al*, 2007; Sloan *et al*, 2014). Although RML-3 homologs in bacteria, including in *Chlamydiales* (Fig 1C), often reside in a chromosomal operon with other rhamnose biosynthetic enzymes, it is also possible that factors that facilitate bacterial HGT, including plasmids and other mobile genetic elements, may have contributed to iHGT. In addition, recent data indicate that virus-like or transposon-mediated gene transfer may occur in nematodes, suggesting that these genetic elements could be an additional contributing factor to this evolutionarily important mechanism of functional innovation (Dennis *et al*, 2012; Moore *et al*, 2021; Widen *et al*, 2023).

How do RML-3 and the acquired capacity to generate L-rhamnose contribute to fitness benefits in nematodes? Our expression and functional analyses of *rml-3* in *C. elegans* demonstrate its critical role in conferring cuticle integrity and organismal resilience against environmental stresses. As a naturally occurring sugar widely distributed among bacteria and plants, L-rhamnose can act as a versatile building block in composite biomolecules, including

rhamnolipids, extracellular polysaccharides, and glycosylated flagella (Wild *et al*, 1997; Gao *et al*, 2001; Schirm *et al*, 2004). These L-rhamnose conjugated biomolecules with altered physical–chemical properties can protect organisms against environmental stresses, such as those from pathogen infection or toxin infiltration. Given the striking cuticle defect and organismal sensitivity to BA in RML-3 deficient *C. elegans*, we propose that L-rhamnose is conjugated to biomolecule target(s) that are critical for cuticle integrity and protection against environmental stresses. While the complete loss of RML-3 causes larval arrest with severe cuticle defects, the partial loss of RML-3 allows larval developmental progression, yet with impaired cuticle leading to BA sensitivity and activation of a cuticle stress-responding pathway for *nlp-29* upregulation. The L-rhamnose conjugated biomolecules critical for cuticle integrity remain to be identified and investigated. Leading candidates include extracellular biomolecules such as collagen, cuticulin, and peptidoglycan, which have been previously implicated in conferring cuticle integrity and resilience to stress (Johnstone, 1994; Ewald *et al*, 2015; Li Zheng *et al*, 2020; Sandhu *et al*, 2021).

In summary, our study reveals the evolutionary origin and organismal role of an L-rhamnose biosynthetic enzyme RML-3 that was acquired from bacteria via iHGT and domesticated in nematodes. With the role in conferring resilience to nematodes against environmental stresses, *rml-3* adds to the growing repertoire of HGTs from microbial species in the *C. elegans* and nematode genomes, including our recent discovery of cyanide detoxification enzymes in *C. elegans* evolutionarily acquired from ancient green algae (Wang *et al*, 2022). Our work supports the emerging notion that the domestication of bacterial genes by iHGT is more widespread in shaping metazoan evolution than currently appreciated and can provide diverse functional capabilities to specific metazoan lineages because of constant and ubiquitous exposure to bacteria. Although rare, iHGT events have had a profound impact on metazoan evolution, as highlighted by the essential roles of RML-3 in modern nematodes to enable exoskeleton integrity, organismal resilience, and survival under adverse environmental conditions.

Materials and Methods

Phylogenetic analysis

C. elegans RML-3 (accession NP_509046.1) was used to query the NCBI RefSeq protein database using BLASTp (Altschul *et al*, 1990) with an e-value cutoff of 1e-5 to obtain the top 5,000 eukaryotic and prokaryotic RML-3 homologs. Additional nematode sequences were obtained by querying the NCBI non-redundant (NR) database using BLASTp for all nematodes or the transcriptome shotgun assembly (TSA) database using tBLASTn for nematodes outside the *Rhabditina*, *Tylenchina*, and *Spirulina* clades that were already well covered from protein searches. The resulting sequences are listed in Dataset EV1. The resulting sequences were aligned using Clustal Omega (Sievers & Higgins, 2014) using two iterations of refinement. Incomplete sequences and poorly aligned proteins were removed from subsequent analyses. To eliminate closely related sequences and reduce the total sequence number, sequences with > 95% identity were reduced to a single unique sequence using CD-HIT with a 0.95 sequence identity cutoff (Fu *et al*, 2012). Following realignment

with Clustal Omega, alignment positions in which > 90% of all sequences had a gap were removed.

IQ-TREE (Nguyen *et al*, 2015) phylogenies were generated using the "-bb 1000 -alrt 1000" commands for the generation of 1,000 ultra-fast bootstrap and SH-aLRT support values. The best-fitting substitution model was determined by ModelFinder (Kalyaanamoorthy *et al*, 2017) using the "-m AUTO" command or the substitution model was specified as shown in Appendix Fig S2 using the "-m" command. FastTree (Price *et al*, 2009) (version 2.1.11) phylogenies were generated using 20 rate categories. All Newick-formatted phylogenetic trees generated from IQ-TREE and FastTree, with support values, can be found in Dataset EV2. Protein phylogenies were visualized as unrooted trees using FigTree (http://tree.bio.ed.ac.uk/software/figtree/).

RML-4 database searches were performed using residues 335–631 of *C. elegans* RML-4 (accession NP_001040727.1). Homologs were obtained by querying the RefSeq (bacteria and eukaryotes) or NR (viruses) databases, using an e-value cutoff of 1e-5. Alignments were generated and refined as above, using the same 95% sequence identity cutoff to remove near-redundant sequences. A maximum likelihood phylogenetic tree was generated using IQ-TREE and ModelFinder as above. A complete Newick-formatted phylogenetic tree with support values can be found in Dataset EV2. Eukaryotic RML-1 homologs were identified using *C. elegans* RML-1 (accession NP_499842.1) and searched against the eukaryotic RefSeq database using BLASTP.

C. elegans culture and transgene construction

All the *C. elegans* strains used in this study were maintained in accordance with the standard laboratory procedures unless otherwise stated (Brenner, 1974). The worms were grown on an OP50 *Escherichia coli* strain at 20°C. Embryos were isolated through sodium hypochlorite treatment. RNAi exposure was performed according to the standard procedure (Kamath & Ahringer, 2003). Strain numbers with genotypes used are: N2 Bristol strain (wild type), DMS2236 *rml-3*(*ust428*), DMS2237 *rml-3*(*ust429*), DMS2233 *rml-3*(*ust430*[*rml-3::gfp::3xflag*]), CB7448 *bus-5*(*e3133*), TP12 *kaIs12* [*col-19::GFP*], DMS2226 *dmaIs145* [*rml-3*p::GFP; *unc-54*p::*mCherry*], XW18042 *qxIs722* [*dpy-7*p::*dpy-7::SfGFP* (single copy)], IG274 *frIs7* [*nlp-29*p::GFP + *col-12*p::*dsRed*].

For constructing *rml-3* transcriptional reporter, GFP-3′UTR was PCR amplified using primers (5′-AGCTTGCATGCCTGCAGGTCG-3′ and 5′-AAGGGCCCGTACGGCCGACTA-3′) and plasmid pPD95.75 (Plasmid #1494- Addgene) as the template. Then, *rml-3* gene-specific primers (Forward 5′-taggtcaaaagtgctggtggc-3′; Reverse 5′-cgacctgcaggcatgcaagcttattcaatgcgagtcaggcaagaa-3′, with sequence immediately upstream of the protein-coding region so that 5′UTR is part of the transgene) were amplified by PCR using a genomic DNA template. Nested PCR was used to generate the gene promoter-GFP fusion product. The fusion product was injected at 20 ng/μl with unc-54::mCherry co-injection marker at 10 ng/μl. The integration of the extrachromosomal arrays was performed through ultraviolet irradiation and backcrossed three to six times.

CRISPR/Cas9-mediated GFP knock-in and gene deletion of *rml-3*

For CRISPR knock-in at the endogenous *rml-3* locus with 3xFLAG:: GFP, a 3xFLAG::GFP region was PCR amplified with the primers

5′-ATGGACTACAAAGACCATGACGG-3′ and 5′-AGCTCCACCTCCA CCTCCTTTG-3′ from the genomic DNA of 3xFLAG::GFP::RPOA-2. A 1.5 kb homologous left arm was PCR amplified with the primers 5′-GGGTAACGCCAGCACGTGTGCGTACTTCGGTCGTGAAATT-3′ and 5′-TCATGGTCTTTGTAGTCCATAGTAGGATGCGACATTATTCAAT-3′. A 1.5 kb homologous right arm was PCR amplified with the primers 5′- AAGGAGGTGGAGGTGGAGCTATGTCGCATCCTACTCCAG-3′ and 5′- CAGCGGATAACAATTTCACAGCGGTGCATCTTCACATTA-3′. The backbone was PCR amplified from the plasmid pCFJ151 with the primers 5′-CACACGTGCTGGCGTTACC-3′ and 5′-TGTGAAATTGTTA TCCGCTGG-3′. All these fragments were joined together by a Gibson assembly to form the 3xFLAG::gfp::*rml-3* plasmid with the ClonExpress MultiS One Step Cloning Kit (Vazyme Biotech). This plasmid was coinjected into N2 animals with three sgRNA expression vectors: *rml-3*_sgRNA#1, *rml-3*_sgRNA#2, *rml-3*_sgRNA#3, 5 ng/μl pCFJ90, and 50 ng/μl Cas9 II expressing plasmid.

To construct sgRNA expression plasmids for CRISPR-mediated *rml-3* deletion, the 20 bp *unc-119* sgRNA guide sequence in the pU6::unc-119 sgRNA(F + E) vector was replaced with different sgRNA guide sequences. Addgene plasmid #47549 was used to express the Cas9 II protein. A plasmid mixture containing 30 ng/μl of each of the three sgRNA expression vectors, 50 ng/μl Cas9 II expressing plasmid, and 5 ng/μl pCFJ90 was co-injected into animals. The deletion mutants were screened by PCR amplification and confirmed by genotyping (Appendix Fig S2).

Epifluorescence microscopy

The epifluorescence compound microscope (Leica DM5000 B Automated Upright Microscope System with 10× and 20× objective lens) and confocal microscope (Leica TCS SPE with a 63× objective lens) were used to capture fluorescence images. Briefly, the synchronous worm population was used for imaging at different developmental stages of indicated genotypes or treated with different RNAi that were randomly picked and anesthetized with 10 mM sodium azide in M9 solution (Sigma-Aldrich) on 2% agar pads on slides. The control and treatment groups were imaged under identical settings and conditions. For the thermal stress assay, the worms were subjected to heat stress at various temperatures (30, 35, and 37°C) with respect to control worms at 20°C prior to imaging. The percentage of cuticle damage was scored in accordance with disruption in the worm cuticles with respect to the control worms (*N* > 50). The rescue of cuticle damage was tested post supplementation of worms with 5–10 mg/ml of L-rhamnose (Fisher, 10030-85-0) and the vehicle control (M9 buffer).

Boric acid sensitivity and rescue assay

BA (Fisher, S25202A) dissolved at 6 mM in the Nematode Growth Medium (NGM) was used for developmental delay studies and 20 mM for survival analysis. For developmental effect studies, control and *rml-3* RNAi-treated L1 were exposed to BA and then imaged on the 6th day of adulthood post L4 stages. For survival analysis, the strains were exposed to BA from the L1 larval stage and the percentage survival was scored either through the last worm surviving with RNAi treatment or post 3 days of exposure in mutants with their respective controls. 10 mg/ml L-rhamnose dissolved in the M9 buffer spread on NGM was used for the rescue assay.

Statistics and reproducibility

Data were analyzed using GraphPad Prism 9.2.0 Software (Graphpad, San Diego, CA) and presented as means $\pm$ SD unless otherwise specified, with significance P values calculated by non-parametric tests or unpaired two-sided t-tests (comparisons between two groups), one-way ANOVA (comparisons across more than two groups) and adjusted with multiple comparison corrections. The lifespan assay was quantified using Kaplan–Meier lifespan analysis, and P-values were calculated using the log-rank test with each experiment reproduced in at least three independent trials.

Data availability

This study includes no data deposited in external repositories.

Expanded View for this article is available online.

Author contributions

Dengke K Ma: Conceptualization; formal analysis; supervision; funding acquisition; investigation; writing – original draft; project administration; writing – review and editing. **Taruna Pandey:** Data curation; formal analysis; investigation; visualization; methodology; writing – review and editing. **Chinmay A Kalluraya:** Formal analysis; investigation; methodology; writing – review and editing. **Bingying Wang:** Data curation; formal analysis; investigation; methodology. **Ting Xu:** Data curation; formal analysis; investigation; methodology. **Xinya Huang:** Data curation; formal analysis; investigation; methodology. **Shouhong Guang:** Data curation; formal analysis; investigation; methodology. **Matthew D Daugherty:** Conceptualization; resources; data curation; software; formal analysis; supervision; funding acquisition; investigation; visualization; methodology; writing – original draft; writing – review and editing.

Disclosure and competing interests statement

The authors declare that they have no conflict of interest.

References

Altschul SF, Gish W, Miller W, Myers EW, Lipman DJ (1990) Basic local alignment search tool. *J Mol Biol* 215: 403–410

Bayramova F, Jacquier N, Greub G (2018) Insight in the biology of *Chlamydia*-related bacteria. *Microbes Infect* 20: 432–440

Bernheim A, Millman A, Ofir G, Meitav G, Avraham C, Shomar H, Rosenberg MM, Tal N, Melamed S, Amitai G *et al* (2021) Prokaryotic viperins produce diverse antiviral molecules. *Nature* 589: 120–124

Blaxter ML, De Ley P, Garey JR, Liu LX, Scheldeman P, Vierstraete A, Vanfleteren JR, Mackey LY, Dorris M, Frisse LM *et al* (1998) A molecular evolutionary framework for the phylum Nematoda. *Nature* 392: 71–75

Brenner S (1974) The genetics of *Caenorhabditis elegans*. *Genetics* 77: 71–94

Brunquell J, Morris S, Lu Y, Cheng F, Westerheide SD (2016) The genome-wide role of HSF-1 in the regulation of gene expression in *Caenorhabditis elegans*. *BMC Genomics* 17: 559

Chandler LM, Choe KP (2022) Extracellular matrix regulation of stress response genes during larval development in Caenorhabditis elegans. *G3 (Bethesda)* 12: jkac221

Chou S, Daugherty MD, Peterson SB, Biboy J, Yang Y, Jutras BL, Fritz-Laylin LK, Ferrin MA, Harding BN, Jacobs-Wagner C *et al* (2015) Transferred interbacterial antagonism genes augment eukaryotic innate immune function. *Nature* 518: 98–101

Crisp A, Boschetti C, Perry M, Tunnacliffe A, Micklem G (2015) Expression of multiple horizontally acquired genes is a hallmark of both vertebrate and invertebrate genomes. *Genome Biol* 16: 50

Danchin EGJ, Rosso M-N, Vieira P, de Almeida-Engler J, Coutinho PM, Henrissat B, Abad P (2010) Multiple lateral gene transfers and duplications have promoted plant parasitism ability in nematodes. *Proc Natl Acad Sci USA* 107: 17651–17656

Dasgupta M, Shashikanth M, Gupta A, Sandhu A, De A, Javed S, Singh V (2020) NHR-49 transcription factor regulates immunometabolic response and survival of *Caenorhabditis elegans* during *Enterococcus faecalis* infection. *Infect Immun* 88: e00130-20

Dennis S, Sheth U, Feldman JL, English KA, Priess JR (2012) *C. elegans* germ cells show temperature and age-dependent expression of Cer1, a Gypsy/Ty3-related retrotransposon. *PLoS Pathog* 8: e1002591

Dunning Hotopp JC (2011) Horizontal gene transfer between bacteria and animals. *Trends Genet* 27: 157–163

Dunning Hotopp JC, Clark ME, Oliveira DCSG, Foster JM, Fischer P, Muñoz Torres MC, Giebel JD, Kumar N, Ishmael N, Wang S *et al* (2007) Widespread lateral gene transfer from intracellular bacteria to multicellular eukaryotes. *Science* 317: 1753–1756

Elwell C, Mirrashidi K, Engel J (2016) Chlamydia cell biology and pathogenesis. *Nat Rev Microbiol* 14: 385–400

Ewald CY, Landis JN, Porter Abate J, Murphy CT, Blackwell TK (2015) Dauer-independent insulin/IGF-1-signalling implicates collagen remodelling in longevity. *Nature* 519: 97–101

Feng L, Shou Q, Butcher RA (2016) Identification of a dTDP-rhamnose biosynthetic pathway that oscillates with the molting cycle in *Caenorhabditis elegans*. *Biochem J* 473: 1507–1521

Ferguson LC, Green J, Surridge A, Jiggins CD (2011) Evolution of the insect yellow gene family. *Mol Biol Evol* 28: 257–272

Fielenbach N, Antebi A (2008) C. elegans dauer formation and the molecular basis of plasticity. *Genes Dev* 22: 2149–2165

Fu L, Niu B, Zhu Z, Wu S, Li W (2012) CD-HIT: accelerated for clustering the next-generation sequencing data. *Bioinformatics* 28: 3150–3152

Gao M, D'Haeze W, De Rycke R, Wolucka B, Holsters M (2001) Knockout of an azorhizobial dTDP-L-rhamnose synthase affects lipopolysaccharide and extracellular polysaccharide production and disables symbiosis with *Sesbania rostrata*. *Mol Plant Microbe Interact* 14: 857–866

Giraud MF, Naismith JH (2000) The rhamnose pathway. *Curr Opin Struct Biol* 10: 687–696

Gravato-Nobre MJ, Nicholas HR, Nijland R, O'Rourke D, Whittington DE, Yook KJ, Hodgkin J (2005) Multiple genes affect sensitivity of *Caenorhabditis elegans* to the bacterial pathogen *Microbacterium nematophilum*. *Genetics* 171: 1033–1045

Haag ES, Fitch DHA, Delattre M (2018) From 'the worm' to 'the worms' and back again: the evolutionary developmental biology of nematodes. *Genetics* 210: 397–433

van den Hoogen J, Geisen S, Routh D, Ferris H, Traunspurger W, Wardle DA, de Goede RGM, Adams BJ, Ahmad W, Andriuzzi WS *et al* (2019) Soil nematode abundance and functional group composition at a global scale. *Nature* 572: 194–198

Husnik F, McCutcheon JP (2018) Functional horizontal gene transfer from bacteria to eukaryotes. *Nat Rev Microbiol* 16: 67–79

Jiang W, Wei Y, Long Y, Owen A, Wang B, Wu X, Luo S, Dang Y, Ma DK (2018) A genetic program mediates cold-warming response and promotes stress-induced phenoptosis in *C. elegans. Elife* 7: e35037

Jiang N, Dillon FM, Silva A, Gomez-Cano L, Grotewold E (2021) Rhamnose in plants – from biosynthesis to diverse functions. *Plant Sci* 302: 110687

Johnstone IL (1994) The cuticle of the nematode *Caenorhabditis elegans*: a complex collagen structure. *Bioessays* 16: 171–178

Kalluraya CA, Weitzel AJ, Tsu BV, Daugherty MD (2023) Bacterial origin of a key innovation in the evolution of the vertebrate eye. *Proc Natl Acad Sci* 120: e2214815120

Kalyaanamoorthy S, Minh BQ, Wong TKF, von Haeseler A, Jermiin LS (2017) ModelFinder: fast model selection for accurate phylogenetic estimates. *Nat Methods* 14: 587–589

Kamath RS, Ahringer J (2003) Genome-wide RNAi screening in *Caenorhabditis elegans. Methods* 30: 313–321

Kiesche-Nesselrodt A, Hooser SB (1990) Toxicology of selected pesticides, drugs, and chemicals. Boric acid. *Vet Clin North Am Small Anim Pract* 20: 369–373

Kondo N, Nikoh N, Ijichi N, Shimada M, Fukatsu T (2002) Genome fragment of Wolbachia endosymbiont transferred to X chromosome of host insect. *Proc Natl Acad Sci USA* 99: 14280–14285

Li Zheng S, Adams JG, Chisholm AD (2020) Form and function of the apical extracellular matrix: new insights from *Caenorhabditis elegans*, *Drosophila melanogaster*, and the vertebrate inner ear. *Fac Rev* 9: 27

Li S, Chen F, Li Y, Wang L, Li H, Gu G, Li E (2022) Rhamnose-containing compounds: biosynthesis and applications. *Molecules* 27: 5315

Luan J-B, Chen W, Hasegawa DK, Simmons AM, Wintermantel WM, Ling K-S, Fei Z, Liu S-S, Douglas AE (2015) Metabolic coevolution in the bacterial symbiosis of whiteflies and related plant sap-feeding insects. *Genome Biol Evol* 7: 2635–2647

Ma DK, Li Z, Lu AY, Sun F, Chen S, Rothe M, Menzel R, Sun F, Horvitz HR (2015) Acyl-CoA dehydrogenase drives heat adaptation by sequestering fatty acids. *Cell* 161: 1152–1163

Martinez V, Ingwers M, Smith J, Glushka J, Yang T, Bar-Peled M (2012) Biosynthesis of UDP-4-keto-6-deoxyglucose and UDP-rhamnose in pathogenic fungi *Magnaporthe grisea* and *Botryotinia fuckeliana. J Biol Chem* 287: 879–892

Mayer WE, Schuster LN, Bartelmes G, Dieterich C, Sommer RJ (2011) Horizontal gene transfer of microbial cellulases into nematode genomes is associated with functional assimilation and gene turnover. *BMC Evol Biol* 11: 13

McGill LM, Shannon AJ, Pisani D, Félix M-A, Ramløv H, Dix I, Wharton DA, Burnell AM (2015) Anhydrobiosis and freezing-tolerance: adaptations that facilitate the establishment of *Panagrolaimus* nematodes in polar habitats. *PloS One* 10: e0116084

Metcalf JA, Funkhouser-Jones LJ, Brileya K, Reysenbach A-L, Bordenstein SR (2014) Antibacterial gene transfer across the tree of life. *Elife* 3: e04266

Mistou M-Y, Sutcliffe IC, van Sorge NM (2016) Bacterial glycobiology: rhamnose-containing cell wall polysaccharides in Gram-positive bacteria. *FEMS Microbiol Rev* 40: 464–479

Moore RS, Kaletsky R, Lesnik C, Cota V, Blackman E, Parsons LR, Gitai Z, Murphy CT (2021) The role of the Cer1 transposon in horizontal transfer of transgenerational memory. *Cell* 184: 4697–4712.e18

Morehouse BR, Govande AA, Millman A, Keszei AFA, Lowey B, Ofir G, Shao S, Sorek R, Kranzusch PJ (2020) STING cyclic dinucleotide sensing originated in bacteria. *Nature* 586: 429–433

Naim N, Amrit FRG, Ratnappan R, DelBuono N, Loose JA, Ghazi A (2021) Cell nonautonomous roles of NHR-49 in promoting longevity and innate immunity. *Aging Cell* 20: e13413

Nguyen L-T, Schmidt HA, von Haeseler A, Minh BQ (2015) IQ-TREE: a fast and effective stochastic algorithm for estimating maximum-likelihood phylogenies. *Mol Biol Evol* 32: 268–274

Parakkottil Chothi M, Duncan GA, Armirotti A, Abergel C, Gurnon JR, Van Etten JL, Bernardi C, Damonte G, Tonetti M (2010) Identification of an L-rhamnose synthetic pathway in two nucleocytoplasmic large DNA viruses. *J Virol* 84: 8829–8838

Pauchet Y, Heckel DG (2013) The genome of the mustard leaf beetle encodes two active xylanases originally acquired from bacteria through horizontal gene transfer. *Proc Biol Sci* 280: 20131021

Price MN, Dehal PS, Arkin AP (2009) FastTree: computing large minimum evolution trees with profiles instead of a distance matrix. *Mol Biol Evol* 26: 1641–1650

Pujol N, Zugasti O, Wong D, Couillault C, Kurz CL, Schulenburg H, Ewbank JJ (2008) Anti-fungal innate immunity in *C. elegans* is enhanced by evolutionary diversification of antimicrobial peptides. *PLoS Pathog* 4: e1000105

Rodriguez M, Snoek LB, De Bono M, Kammenga JE (2013) Worms under stress: *C. elegans* stress response and its relevance to complex human disease and aging. *Trends Genet* 29: 367–374

Rota-Stabelli O, Daley AC, Pisani D (2013) Molecular timetrees reveal a Cambrian colonization of land and a new scenario for ecdysozoan evolution. *Curr Biol* 23: 392–398

Sandhu A, Badal D, Sheokand R, Tyagi S, Singh V (2021) Specific collagens maintain the cuticle permeability barrier in *Caenorhabditis elegans. Genetics* 217: iyaa047

Schiffer PH, Danchin EGJ, Burnell AM, Creevey CJ, Wong S, Dix I, O'Mahony G, Culleton BA, Rancurel C, Stier G *et al* (2019) Signatures of the evolution of parthenogenesis and cryptobiosis in the genomes of panagrolaimid nematodes. *iScience* 21: 587–602

Schirm M, Arora SK, Verma A, Vinogradov E, Thibault P, Ramphal R, Logan SM (2004) Structural and genetic characterization of glycosylation of type a flagellin in *Pseudomonas aeruginosa. J Bacteriol* 186: 2523–2531

Scholl EH, Thorne JL, McCarter JP, Bird DM (2003) Horizontally transferred genes in plant-parasitic nematodes: a high-throughput genomic approach. *Genome Biol* 4: R39

Schönknecht G, Chen W-H, Ternes CM, Barbier GG, Shrestha RP, Stanke M, Bräutigam A, Baker BJ, Banfield JF, Garavito RM *et al* (2013) Gene transfer from bacteria and archaea facilitated evolution of an extremophilic eukaryote. *Science* 339: 1207–1210

Sievers F, Higgins DG (2014) Clustal Omega, accurate alignment of very large numbers of sequences. *Methods Mol Biol* 1079: 105–116

Sinner MP, Masurat F, Ewbank JJ, Pujol N, Bringmann H (2021) Innate immunity promotes sleep through epidermal antimicrobial peptides. *Curr Biol* 31: 564–577

Sloan DB, Nakabachi A, Richards S, Qu J, Murali SC, Gibbs RA, Moran NA (2014) Parallel histories of horizontal gene transfer facilitated extreme reduction of endosymbiont genomes in sap-feeding insects. *Mol Biol Evol* 31: 857–871

Smythe AB, Holovachov O, Kocot KM (2019) Improved phylogenomic sampling of free-living nematodes enhances resolution of higher-level nematode phylogeny. *BMC Evol Biol* 19: 121

Sommer RJ, Bumbarger DJ (2012) Nematode model systems in evolution and development. *Wiley Interdiscip Rev Dev Biol* 1: 389–400

Taubert S, Hansen M, Van Gilst MR, Cooper SB, Yamamoto KR (2008) The Mediator subunit MDT-15 confers metabolic adaptation to ingested material. *PLoS Genet* 4: e1000021

Thein MC, McCormack G, Winter AD, Johnstone IL, Shoemaker CB, Page AP (2003) *Caenorhabditis elegans* exoskeleton collagen COL-19: an adult-specific marker for collagen modification and assembly, and the analysis of organismal morphology. *Dev Dyn* 226: 523–539

Verster KI, Wisecaver JH, Karageorgi M, Duncan RP, Gloss AD, Armstrong EE, Price DK, Menon AR, Ali ZM, Whiteman NK (2019) Horizontal transfer of bacterial cytolethal distending toxin B genes to insects. *Mol Biol Evol* 36: 2105–2110

Vozdek R, Long Y, Ma DK (2018) The receptor tyrosine kinase HIR-1 coordinates HIF-independent responses to hypoxia and extracellular matrix injury. *Sci Signal* 11: eaat0138

Wang B, Pandey T, Long Y, Delgado-Rodriguez SE, Daugherty MD, Ma DK (2022) Co-opted genes of algal origin protect *C. elegans* against cyanogenic toxins. *Curr Biol* 32: 4941–4948

Wheeler D, Redding AJ, Werren JH (2013) Characterization of an ancient lepidopteran lateral gene transfer. *PLoS One* 8: e59262

Widen SA, Bes IC, Koreshova A, Pliota P, Krogull D, Burga A (2023) Virus-like transposons cross the species barrier and drive the evolution of genetic incompatibilities. *Science* 380: eade0705

Wild M, Caro AD, Hernández AL, Miller RM, Soberón-Chávez G (1997) Selection and partial characterization of a *Pseudomonas aeruginosa* mono-rhamnolipid deficient mutant. *FEMS Microbiol Lett* 153: 279–285

Wybouw N, Dermauw W, Tirry L, Stevens C, Grbić M, Feyereisen R, Van Leeuwen T (2014) A gene horizontally transferred from bacteria protects arthropods from host plant cyanide poisoning. *Elife* 3: e02365

Xiong H, Pears C, Woollard A (2017) An enhanced *C. elegans* based platform for toxicity assessment. *Sci Rep* 7: 9839

Zhang Z, Bai M, Barbosa GO, Chen A, Wei Y, Luo S, Wang X, Wang B, Tsukui T, Li H *et al* (2020) Broadly conserved roles of TMEM131 family proteins in intracellular collagen assembly and secretory cargo trafficking. *Sci Adv* 6: eaay7667

Zhang Z, Luo S, Barbosa GO, Bai M, Kornberg TB, Ma DK (2021) The conserved transmembrane protein TMEM-39 coordinates with COPII to promote collagen secretion and regulate ER stress response. *PLoS Genet* 17: e1009317

Zhaxybayeva O, Doolittle WF (2011) Lateral gene transfer. *Curr Biol* 21: R242–R246